Research article

Kyoung-Duck Park, Minh Tan Man, Deok-Yong Cho and Hong Seok Lee*

Wide-gap photoluminescence control of quantum dots through atomic interdiffusion and bandgap renormalization

https://doi.org/10.1515/nanoph-2020-0482
Received August 22, 2020; accepted October 8, 2020;
published online October 29, 2020

Abstract: Bandgap and photoluminescence (PL) energy control of epitaxially grown II–VI quantum dots (QDs) are highly desirable for applications in optoelectronic devices, yet little work has been reported. Here, we present a wide tunability of PL emission for CdTe/ZnTe QDs through an impurity-free vacancy disordering method. To induce compressive stress at the dielectric layer/ZnTe interface, a SiO_2 film is deposited onto the samples, followed by rapid thermal annealing to induce atomic interdiffusion. After the heat treatment, the PL spectra of the intermixed QDs show pronounced blueshifts in peak energy as large as ~200 meV because of the reduced bandgap renormalization and decreased quantum confinement effects in addition to the dominant atomic interdiffusion effect. In addition, we present a thorough investigation on the modified physical properties of the intermixed QDs, including their lattice structure, thermal escape energy, and carrier dynamics, through quantitative X-ray and optical characterizations.

Keywords: atomic interdiffusion; bandgap renormalization; carrier dynamics; quantum dots; thermal escape energy.

***Corresponding author: Hong Seok Lee**, Department of Physics, Research Institute of Physics and Chemistry, Jeonbuk National University, Jeonju 54896, Republic of Korea,
E-mail: hslee1@jbnu.ac.kr. https://orcid.org/0000-0002-1292-0731
Kyoung-Duck Park, Department of Physics, Ulsan National Institute of Science and Technology (UNIST), Ulsan 44919, Republic of Korea. https://orcid.org/0000-0002-9302-9384
Minh Tan Man, Institute of Theoretical and Applied Research, Duy Tan University, Hanoi 100000, Vietnam; and Faculty of Natural Sciences, Duy Tan University, Da Nang 550000, Vietnam
Deok-Yong Cho, IPIT & Department of Physics, Jeonbuk National University, Jeonju 54896, Republic of Korea

1 Introduction

Low-dimensional nanostructures of light-emitting semiconductors, e.g., two-dimensional (2D) multiquantum wells [1, 2], one-dimensional (1D) quantum wires [3, 4], zero-dimensional (0D) quantum dots (QDs) [5, 6], and even atomic sheets [7, 8], have emerged as appealing optical sources for next-generation optoelectronic technologies. Specifically, QDs are becoming increasingly important as a key building block for high-performance devices such as displays [9, 10], photovoltaics [11, 12], photocatalysts [13, 14], and quantum information processors [15, 16] because of their high extinction coefficient and single quantum emitting behaviors [17, 18]. Chemically synthesized colloidal QDs enable the fabrication of bright displays and highly efficient photocatalysts [9, 10, 13, 14]. However, because they are mainly used in the form of an ensemble, the precise positioning and regulation of the number of particles on the device are challenging. By contrast, epitaxial growth techniques enable precise control of the QD location [19] as well as the dipole orientation [20], even at the single-particle level [21]. Therefore, epitaxially grown QDs are attracting much attention for on-chip architectures of a range of solid-state devices [22–24]. For example, monolithic integration of bandgap tunable QD devices is highly desirable for optical communication systems [25], yet controlling the bandgap and emission energy over a broad spectral range remains a substantial challenge.

Previously, efforts to develop bandgap-tuning methods have led to several different approaches, including laser-induced intermixing [26], impurity-induced disordering [27], plasma-assisted induced disordering [28], impurity-free vacancy disordering (IFVD) [29]. IFVD is a well-known method of promoting atomic intermixing by inducing compressive or tensile strain at the interface of semiconducting nanostructures. This approach is particularly attractive because it does not rely on ion implantation, which introduces impurities into the crystal lattice [30, 31]. Thus far, most studies on QD

intermixing have focused on various III–V QDs [26, 32, 33]; by contrast, few works on epitaxial II–VI QDs have been reported even though they exhibit superior excitonic properties as a result of their large exciton binding energy, e.g., wide-gap CdTe/ZnTe QDs in the green-orange spectral region [34]. In addition, a thorough investigation of the modified physical properties of intermixed QDs has not yet been reported.

In the present work, we demonstrate systematic bandgap and photoluminescence (PL) energy control for CdTe/ZnTe QDs through IFVD-based atomic intermixing. Under the optimized annealing temperature and time as well as optimized thickness of the dielectric capping layer, we achieve a PL peak shift as large as ~200 meV ranging from 2.1 to 2.3 eV. In addition, we demonstrate quantitative X-ray and optical characterizations to elucidate the modified properties of QDs, such as their lattice structure, carrier dynamics, and thermal escape energy, before and after the QD intermixing. This work presents a generalizable method for wavelength-tunable II–VI QD devices and provides a guideline for investigating their structural, optical, and electronic properties.

2 Experiment

2.1 Sample preparation

The CdTe QDs were grown on a GaAs (100) substrate via a home-built molecular-beam epitaxy (MBE) and atomic layer epitaxy (ALE) with ZnTe cap layers. The GaAs substrate was degreased in warm trichloroethylene, cleaned with acetone and methanol, and thoroughly rinsed with deionized water. The substrate was then mounted onto a molybdenum susceptor for thermal cleaning immediately after the chemical cleaning processes. After thermal cleaning at 600 °C for 5 min, a 900 nm ZnTe cap layer was grown on the GaAs substrate at 320 °C using MBE, followed by the deposition of 4.0 monolayers (ML) of CdTe at 320 °C via ALE, resulting in the formation of QDs. The density of as-grown CdTe QDs was characterized as ~4×10^{10} cm^{-2} from an atomic force microscopy measurement (see Supplementary materials for details). The CdTe QDs were then capped with a 100 nm-thick ZnTe layer grown at 320 °C using MBE. The Zn and Te source temperatures used in the growth of the ZnTe layer were 280 and 300 °C, respectively. The Cd and Te source temperatures used in the deposition of the CdTe layer were 195 and 300 °C, respectively. One cycle of ALE growth was performed through an optimum growth process in which the Cd effusion cell was opened for 8 s and growth was interrupted for 1 s. Thereafter, the Te effusion cell was opened for 8 s and growth was interrupted for 5 s. The interruption process was used to improve the film quality by stabilizing the positive and negative ions on the surface of the film. Finally, the sample surface was coated with 300 nm-thick SiO_2 by plasma-enhanced chemical vapor deposition. The samples from the same wafer were cut and annealed for 10, 60, 90, and 120 s at 500 °C under a N_2 atmosphere using a rapid thermal processor. These five samples were used for X-ray and optical characterizations in Sections 3.1–3.4.

2.2 Characterizations

2.2.1 Photoluminescence spectroscopy

The samples were excited by 400 nm frequency-doubled femtosecond pulses from a 76 MHz mode-locked Ti:sapphire laser system (MIRA900, Coherent). The PL signal from the samples was dispersed using a 15 cm monochromator and detected by a photomultiplier tube (Princeton Instruments). The sample temperature was varied between 20 and 110 K using a He closed-cycle Displex refrigeration system. Time-resolved PL decay curves were measured using a commercially available time-correlated single photon counting (TCSPC) module with a multichannel plate photomultiplier tube (PicoHarp, PicoQuant GmbH). The full-width at half-maximum (FWHM) of the total instrument response function (IRF) was less than 130 ps. Note that the PL response of QD samples was observed also at room temperature, yet the quantum yield was lower than the PL measurement at low temperatures (see Supplementary materials for details).

2.2.2 X-ray absorption spectroscopy

X-ray absorption spectroscopy (XAS) at the Cd L_3-edge ($h\nu$ = ~3540 eV) was performed at the 16A1 beamline of the Taiwan Light Source using a Lytle fluorescence yield (FY) detector. The angle between the incident X-rays and the sample plane was set to 45°. Because the probe depth of the FY mode exceeds 1 μm at 3540 eV, the absorption signal of Cd ions placed below the 300 nm SiO_2 and 100 nm ZnTe layers was observed successfully. The photon energy was calibrated using the maximal slope in the Pd L_1-edge spectrum ($h\nu$ = ~3604 eV) of a Pd foil.

2.3 Simulations

2.3.1 XAS simulation

The theoretical spectra for the CdTe QDs were obtained using an ab-initio real-space multiple scattering code, FEFF8 [35]. A full multiple scattering within a spherical model cluster containing 87 atoms (which correspond to a radius of ~8.0–8.5 Å depending on the size of the lattices) was calculated for all of the simulated spectra.

3 Results and discussion

3.1 Atomic interdiffusion of CdTe/ZnTe quantum dots

For the II–VI QD-intermixing experiment, 4.0 ML of CdTe QDs were grown on a GaAs (100) substrate with ZnTe buffer layers via MBE and ALE. The as-grown samples were then coated with a dielectric thin film (300 nm-thick SiO_2) by plasma-enhanced chemical vapor deposition, as shown in Figure 1a. To control the PL energy of the CdTe QDs by inducing atomic intermixing between CdTe and the 100 nm ZnTe cap layer, the samples were annealed for various times (10, 60, 90, and 120 s) at 500 °C under a N_2 atmosphere using a rapid thermal processor.

Figure 1b shows the PL spectra measured at 20 K for QDs annealed for different annealing times of 10, 60, 90, and 120 s at 500 °C. The PL peaks of the annealed QDs are blueshifted because of the interdiffusion of Cd and Zn atoms, which is attributed to a difference of the thermal expansion coefficient between SiO_2 (0.52×10^{-6} °C^{-1}) and ZnTe (8.3×10^{-6} °C^{-1}). Specifically, because the thermal expansion coefficient of SiO_2 is much smaller than that of ZnTe, compressive stress is induced at the interface between the ZnTe and SiO_2 layers during annealing. This stress enhances the diffusivity of Zn vacancies in the underlying structure, thereby enabling the interdiffusion of Cd and Zn atoms at the interface between the QDs and the barrier materials, as described in Figure 1a. This atomic intermixing gives rise to a shallow confining potential of the QDs due to the incorporation of more Zn atoms into the CdTe QDs, as described in previous studies on III–V QDs [26, 32, 33].

Our experimental results show that the PL blueshift of the intermixed QD is linearly proportional to the square root of annealing time (Figure 1c). This result is in good agreement with the expression $L_d \propto \sqrt{t_{Anneal}}$ relating the interdiffusion length (L_d) and the annealing time (t_{Anneal}) [36]. From a linear line fitting of the measurement data, we derive the PL peak shift $\Delta_{Peak} \cong \alpha \cdot \sqrt{t_{Anneal}}$, where α is a proportionality constant with a value of $\alpha = 19 \pm 1\,\text{meV}/\sqrt{s}$. It should be noted that the slope α can be changed depending on the annealing conditions. For instance, we obtain the reduced slope $\alpha = 16 \pm 1\,\text{meV}/\sqrt{s}$ in the control experiment performed at 400 °C (see Supplementary materials for details). The observed blueshift, which is as large as ~200 meV, means the initial QD compound of CdTe can be denaturalized into $Cd_xZn_{1-x}Te$ QDs through the interdiffusion process. Note that the maximum tunable range of the annealed QDs is as wide as the bandgap energy of a ZnTe barrier layer (see Supplementary materials for details).

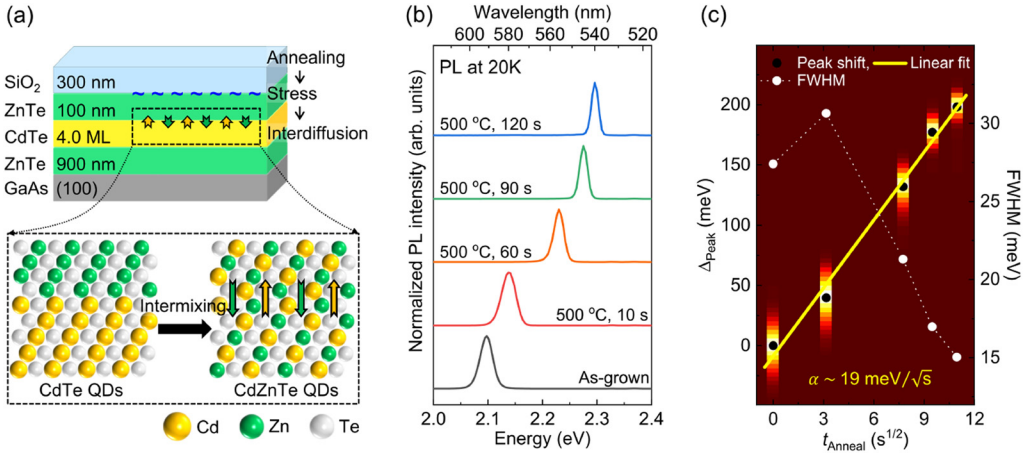

Figure 1: (a) Schematic of the structure of epitaxially grown CdTe/ZnTe QDs with a SiO_2 capping layer and an illustration of QD intermixing via thermal annealing. (b) Normalized low-temperature PL spectra of QD samples with different annealing times. (c) PL peak shift and FWHM of the CdTe/ZnTe QDs with respect to the annealing time. PL spectra of the five samples are shown as background 2D contour images at each peak position. A linear relation between the PL peak shift and the square root of time is shown as a yellow line (slope $\alpha = 19 \pm 1\,\text{meV}/\sqrt{s}$). QD, quantum dot; PL, photoluminescence.

n addition to the expected interdiffusion of Cd and Zn atoms, the larger bandgap of $Cd_xZn_{1-x}Te$ QDs compared with that of CdTe QDs supports this hypothesis [37]. To understand the dependence of the linewidth change on the annealing time, PL spectra of the five samples are also shown as background 2D contour images in Figure 1c. The white dots with a dashed line show the FWHMs of the PL spectra corresponding to as-grown CdTe QDs and the intermixed $Cd_xZn_{1-x}Te$ QDs. With increasing annealing time, the linewidths become narrower except for that of the QD sample annealed for 10 s. In general, the PL linewidth of QD ensemble is associated with a uniformity of QD size. Thus, the observed change in PL linewidth with respect to the annealing time provides information about the heterogeneity of the QD islands. The PL broadening observed for the sample annealed for 10 s indicates a larger degree of heterogeneity in the QD size. As intermixing begins, the smaller QDs in the ensemble have a relatively higher occupation at the CdTe/ZnTe interface compared with the larger QDs. Hence, for a short annealing time, interdiffusion is more significant for the smaller QDs because of the short interdiffusion length. Therefore, the dot-size distribution is quite inhomogeneous in the case of short annealing times. By contrast, for the QDs annealed for longer times, the confining potential becomes shallow, which leads to reduced inhomogeneous broadening in the PL spectrum.

3.2 Atomic structures of the intermixed quantum dots

To characterize the local atomic structures of the Cd^{2+} ions in the intermixed QDs, X-ray absorption near-edge structure (XANES) spectra were measured using synchrotron radiation. Figure 2a shows the experimental XANES results at the Cd L_3-edge for the as-grown and post-annealed QDs; these spectra reveal the coordination of the Cd^{2+} ions. For comparison, the XANES spectrum of a 1 μm-thick CdTe film is also shown. Overall, the measured absorption spectra show similar oscillatory features; however, the period of the oscillations slightly increases with increasing annealing time, as indicated by dashed lines A, B, C, and D. Such oscillatory features above the threshold energy ($h\nu$ = ~3538 eV) are originated from the electron-atom scatterings of the quasi-free electron waves, which are created by Cd $2p_{3/2} \rightarrow 4d$ electron excitation. Thus, the oscillation period is determined by the interatomic distance between the photon-absorbing atom, i.e., Cd, and the neighboring atoms, i.e., Te, Zn, or Cd. That is, the longer period in energy, e.g., the photon energy difference between the positions A and B of the QDs annealed for 120 s, indicates a shorter Cd–Te atomic bond length. Specifically, the CdTe film shows the shortest period of ~6.0 eV with a slightly increased period for the QD structure (0 s), as seen in Figure 2a. By contrast, the postannealed QDs show a gradually increasing period ranging from 6.4 to 7.0 eV depending on the annealing time. These results show that the average bond length between Cd and neighboring atoms is shorter in the QD structure than in the CdTe thin film (2.806 Å). In addition, the results show that a longer annealing time of the QDs results in a shorter bond length due to the atomic intermixing and transformation into $Cd_xZn_{1-x}Te$ QDs.

To analyze the observed oscillatory behaviors quantitatively, we carry out theoretical simulations for model structures of CdTe in the cubic ZnS structure (F-43m). In

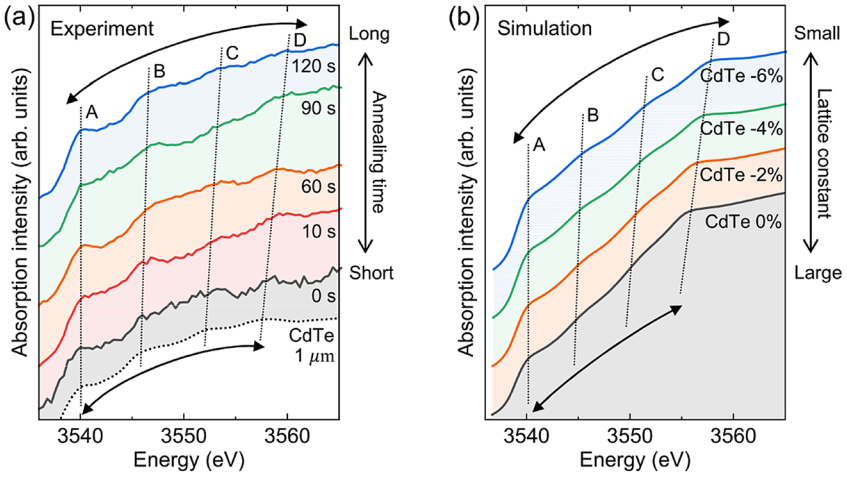

Figure 2: (a) Cd L_3-edge XANES spectra of the CdTe QDs annealed for different times. (b) The XANES simulation results (FEFF8) for a cubic CdTe with various ratios of reduction in Cd–Te bond lengths. Dotted lines A, B, C, and D are visual guides emphasizing the evolution of the separations of the oscillatory features. QD, quantum dot; XANES, X-ray absorption near-edge structure.

this model, the initial lattice constant of Cd–Te bonds is set to 6.48 Å and is gradually reduced to 98, 96, and 94% in the simulation series. The contraction of the lattice constant of Cd–Te to 94%, assuming a case of post-interdiffusion, corresponds to the lattice constant of Zn–Te (6.09 Å). Figure 2b shows the XANES simulation results revealing oscillatory behavior similar to that of the experimental results. The increasing period of the oscillation is clearly shown with respect to the decreasing lattice constant by 0 to –6%. This result shows that bond lengths between Cd and neighboring atoms are shortened with increasing annealing time. On the basis of this simulation result, we estimate that the bond lengths of the intermixed QDs are gradually decreased to ~2.64 Å depending on the annealing time, from the initial Cd–Te bond length of ~2.75 Å for the as-grown QDs. The estimated value of ~2.64 Å (120 s) is approximately the same as the Zn–Te bond length in the ZnTe QDs because the intermixed QDs have a molecular structure of $Cd_xZn_{1-x}Te$ due to the interdiffusion of Cd and Zn atoms, as shown in Figure 1a. Specifically, the substitution of Zn in the annealed QDs induces a ZnTe-like local environment for the Cd ions, i.e., Cd ions will exist as isolated ions in a ZnTe matrix when the annealing time is sufficient. Under this condition, the ZnTe matrix with shorter cation-Te bonds than CdTe will impose a local compressive strain on the CdTe QDs, giving rise to the bandgap increase and PL blueshift, as seen in Figure 1b.

3.3 Bandgap renormalization and thermal escape process

We next perform temperature-dependent PL measurements for a series of samples to understand the carrier redistribution and phonon-induced thermal escape by determining the activated thermal energy. Figure 3a shows PL spectra of the as-grown CdTe QDs and intermixed $Cd_xZn_{1-x}Te$ QDs (t_{Anneal} = 120 s) acquired at different temperatures ranging from 20 to 110 K. Both samples show an anomaly in the emission shift (Figure 3b) and quenching of the PL spectra with increasing temperature, both of which are caused by an inhomogeneous distribution of the localized carriers to escape and diffuse to the trap. For the confined carriers in QDs, tracking the integrated PL intensity as a function of temperature gives access to information about the thermal escape process, which is explained on the basis of the redistribution of carriers in the localization potentials [38]. Therefore, we use a model for the temperature-dependent integrated PL intensity $I_{PL}(T)$ given by Man and Lee [38]

$$I_{PL}(T) = \frac{I(0)}{1 + 2ae^{-\Delta E/k_BT} + 3be^{-2\Delta E/k_BT} + c(e^{E_{LO}/k_BT} - 1)^{-m}} \quad (1)$$

where a, b, and c are constants associated with the relative energy density of states, $I(0)$ is the integrated PL intensity at 0 K, ΔE is the thermal activation energy for the low-temperature quenching processes [38], m is the number of longitudinal-optical (LO) phonons involved in the thermal escape of carriers, and E_{LO} is the average LO phonon energy. We plot the change in the integrated PL intensity as a function of temperature for the five QD samples, with model fitting to Eq. (1). As can be seen in Figure 4a, the QDs with t_{Anneal} = 10 s exhibit the most substantial intensity change and the range of the temperature-dependent intensity shift gradually decreases with increasing t_{Anneal}. From the fitting profiles based on Eq. (1), we derive the thermal activation energy ΔE and the thermal escape energy E_{escape} for a series of samples, as shown in

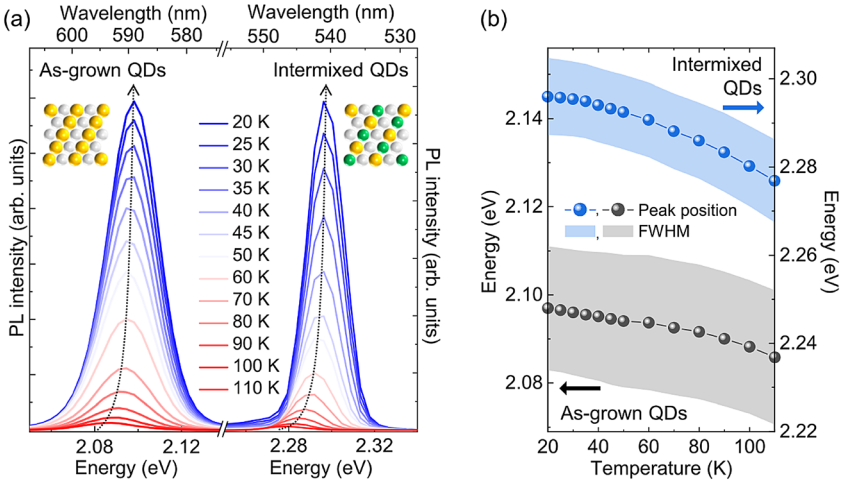

Figure 3: (a) Temperature-dependent PL spectra of the as-grown CdTe QDs and intermixed $Cd_xZn_{1-x}Te$ QDs (t_{Anneal} = 120 s). (b) Plots of the derived emission peak and linewidth change (from Figure 3a) with respect to the measurement temperature. QD, quantum dot; PL, photoluminescence.

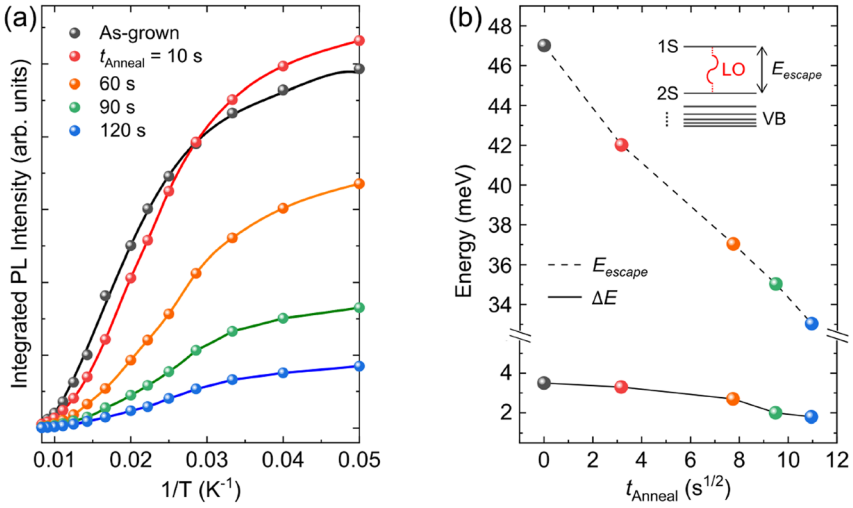

Figure 4: (a) Integrated PL intensity with respect to the measurement temperature for a series of QD samples, along with the model fit profiles (solid lines). (b) Thermal escape energy E_{escape} and thermal activation energy ΔE for the as grown and the intermixed QD samples derived from Figure 4a. E_{escape} in the valence band (VB) is described in the inset. QD, quantum dot; PL, photoluminescence.

Figure 4b. The derived thermal activation energies ΔE clearly decrease from 3.5 to 1.8 meV with increasing annealing time. These quantified energy scales are attributed to the energy separation between the different states at low temperatures which are on the same energy scale as the energy splitting of confined acoustic phonons in QDs. By contrast, the derived thermal escape energy, associated with the quantum efficiency limit at high temperatures, shows a more pronounced decreasing behavior (Figure 4b). The obtained E_{escape} ranging from 33 to 47 meV corresponds to the energy of a few LO phonons, i.e., $E_{escape} = m \cdot E_{LO}$ $(2 \le m \le 3)$. Thus, this result is associated with carrier–carrier scattering for relaxation dynamics [39]. Because the thermal escape energy matches the energy separation of excited states, i.e., the energy difference between the 1S(h) and 2S(h) in the valence band (inset of Figure 4b) [39], longer annealing times lead to a reduced E_{LO} in the intermixed $Cd_xZn_{1-x}Te$ QDs. This quantitative analysis, combined with the observed PL blueshifts (Figure 1b), indicates a reduced bandgap renormalization (BGR) effect as a result of the QD interdiffusion [40]. The BGR effect can be evaluated by an empirical formula $\Delta E_{BGR} = -k \cdot n^{1/3}$ (PL redshift due to the shrinkage of bandgap) because of Coulomb interactions between the free carriers, where k is the BGR coefficient and n is the carrier density [40, 41]. Hence, the reduced BGR effect in the postannealed QDs, by the decreased thermal escape energy and correspondingly reduced carrier density, gives rise to the PL blueshift as high as ~200 meV in our experiment. Note that because the thermal escape energy and the activation energy are decreased after the thermal annealing, the quantum yield of the annealed QDs is lower than the as-grown QDs.

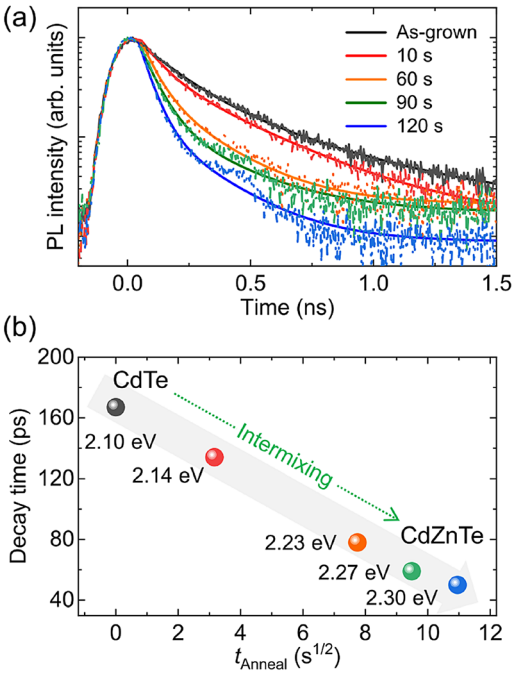

Figure 5: (a) Time-resolved PL spectra for the as-grown and post-annealed QDs measured using a TCSPC module at the PL peak of each sample. Solid lines indicate fitting curves with a biexponential function. (b) PL decay times of QD samples as a function of the annealing time. A linear relation between the decay time and the square root of annealing time is shown as a black line (slope $\alpha = -11 \times 10^{-12}\sqrt{s}$). QD, quantum dot; PL, photoluminescence; TCSPC, time-correlated single photon counting.

3.4 Carrier dynamics of the intermixed quantum dots

We then perform time-resolved PL measurements using the TCSPC method to understand the carrier dynamics properties of the intermixed QDs. Figure 5a shows the time-resolved PL decay curves for the as-grown and postannealed QDs measured at the PL peak of each sample. For the QD samples with longer annealing times, the PL decay time is obviously decreased. To quantify the decay time of each sample, we perform reconvolution fitting with IRF for the measured time-resolved PL spectra and fitting the decay curves with a biexponential function [42]. The decay curves fitted with the biexponential function show fast and slow components associated with the bright and dark excitons [43]. Hereafter, we take only the fast component into account to derive the decay time. To quantify the decay time of each sample, we perform reconvolution fitting with IRF for the measured time-resolved PL spectra [42]. For the as-grown and intermixed QDs annealed for 10, 60, 90, and 120 s at 500 °C, the decay times are derived as $\tau = 167$, 134, 78, 59, and 50 ps, as shown in Figure 5b. This inversely proportional relation between the radiative lifetime and the QD annealing time is associated with the composition change, modified carrier confinement, and the reduced BGR effect. Note that we expect the formation of defects during annealing contributes less to the decreased lifetime because the preserved surface quality and thermal stability with a SiO_2 capping layer can effectively reduce the number of defects in our annealed QDs [44]. From this result, in conjunction with the previously discussed PL characterizations, we conclude that the PL energy blueshift of the annealed QDs is attributable to the atomic interdiffusion as well as the modified carrier confinement and the reduced BGR effect.

4 Conclusions

We demonstrated wide tunability of the PL energy for CdTe/ZnTe QDs through atomic interdiffusion to form $Cd_xZn_{1-x}Te$ QDs. In addition to the dominant interdiffusion effect, the reduced BGR effect with the decreased carrier confinement enables a PL blueshift as large as ~200 meV, from 2.1 eV for the as-grown QDs to 2.3 eV for the intermixed QDs. Our work shows that epitaxial II–VI QDs with the postannealing approach provide a pathway for broad optoelectronic device applications in the visible spectral region. In addition, we demonstrated a series of optical characterization methods, such as XANES, temperature-dependent PL, and time-resolved PL, in conjunction with theoretical models to investigate the modified physical properties of the intermixed QDs, e.g., lattice structure, thermal escape energy, and carrier dynamics. We believe this work provides a guideline for analyzing the correlated structural, electronic, and optical properties of wavelength-tunable semiconducting devices.

Author contribution: All the authors have accepted responsibility for the entire content of this submitted manuscript and approved submission.
Research funding: This research was supported by the Basic Science Research Program through the National Research Foundation of Korea (NRF) funded by the Ministry of Science and ICT (NRF-2018R1A2B6001019). This work was supported by the National Research Foundation of Korea (NRF) grant funded by the Korea government (MEST) (No. 2020R1C1C1011301).
Conflict of interest statement: The authors declare no conflicts of interest regarding this article.

References

[1] C. Weisbuch, R. Dingle, A. C. Gossard, and W. Wiegmann, "Optical characterization of interface disorder in GaAs-$Ga_{1-x}Al_xAs$ multi-quantum well structures," *Solid State Commun.*, vol. 38, no. 8, pp. 709–712, 1981.
[2] S. Nakamura, M. Senoh, S. Nagahama, et al., "Room-temperature continuous-wave operation of InGaN multi-quantum-well structure laser diodes," *Appl. Phys. Lett.*, vol. 69, no. 26, pp. 4056–4058, 1996.
[3] L. Bányai, I. Galbraith, C. Ell, and H. Haug, "Excitons and biexcitons in semiconductor quantum wires," *Phys. Rev. B*, vol. 36, no. 11, p. 6099, 1987.
[4] E. Kapon, D. M. Hwang, and R. Bhat, "Stimulated emission in semiconductor quantum wire heterostructures," *Phys. Rev. Lett.*, vol. 63, no. 4, p. 430, 1989.
[5] T. Takagahara, "Excitonic optical nonlinearity and exciton dynamics in semiconductor quantum dots," *Phys. Rev. B*, vol. 36, no. 17, p. 9293, 1987.
[6] P. M. Petroff and S. P. DenBaars, "MBE and MOCVD growth and properties of self-assembling quantum dot arrays in III-V semiconductor structures," *Superlattices Microstruct.*, vol. 15, no. 1, p. 15, 1994.
[7] A. Splendiani, L. Sun, Y. Zhang, et al., "Emerging photoluminescence in monolayer MoS_2," *Nano Lett.*, vol. 10, no. 4, pp. 1271–1275, 2010.
[8] K. F. Mak, C. Lee, J. Hone, J. Shan, and T. F. Heinz, "Atomically thin MoS_2: a new direct-gap semiconductor," *Phys. Rev. Lett.*, vol. 105, no. 13, p. 136805, 2010.

[9] E. Jang, S. Jun, H. Jang, J. Lim, B. Kim, and Y. Kim, "White-light-emitting diodes with quantum dot color converters for display backlights," *Adv. Mater.*, vol. 22, no. 28, pp. 3076–3080, 2010.
[10] T.-H. Kim, K.-S. Cho, E. K. Lee, et al., "Full-colour quantum dot displays fabricated by transfer printing," *Nat. Photon.*, vol. 5, no. 3, pp. 176–182, 2011.
[11] A. J. Nozik, M. C. Beard, J. M. Luther, M. Law, R. J. Ellingson, and J. C. Johnson, "Semiconductor quantum dots and quantum dot arrays and applications of multiple exciton generation to third-generation photovoltaic solar cells," *Chem. Rev.*, vol. 110, no. 11, pp. 6873–6890, 2010.
[12] J. H. Bang and P. V. Kamat, "Quantum dot sensitized solar cells. A tale of two semiconductor nanocrystals: CdSe and CdTe," *ACS Nano*, vol. 3, no. 6, pp. 1467–1476, 2009.
[13] Y.-F. Xu, M.-Z. Yang, B.-X. Chen, et al., "A $CsPbBr_3$ perovskite quantum dot/graphene oxide composite for photocatalytic CO_2 reduction," *J. Am. Chem. Soc.*, vol. 139, no. 16, pp. 5660–5663, 2017.
[14] S. Saha, G. Das, J. Thote, and R. Banerjee, "Photocatalytic metal–organic framework from CdS quantum dot incubated luminescent metallohydrogel," *J. Am. Chem. Soc.*, vol. 136, no. 42, pp. 14845–14851, 2014.
[15] A. Imamog, D. D. Awschalom, B. Guido, et al., "Quantum information processing using quantum dot spins and cavity QED," *Phys. Rev. Lett.*, vol. 83, no. 20, p. 4204, 1999.
[16] H. J. Krenner, S. Stufler, M. Sabathil, et al., "Recent advances in exciton-based quantum information processing in quantum dot nanostructures," *New J. Phys.*, vol. 7, no. 1, p. 184, 2005.
[17] G. S. Solomon, M. Pelton, and Y. Yamamoto, "Single-mode spontaneous emission from a single quantum dot in a three-dimensional microcavity," *Phys. Rev. Lett.*, vol. 86, no. 17, p. 3903, 2001.
[18] V. Zwiller, H. Blom, P. Jonsson, et al., "Single quantum dots emit single photons at a time: antibunching experiments," *Appl. Phys. Lett.*, vol. 78, no. 17, pp. 2476–2478, 2001.
[19] A. Mohan, M. Felici, P. Gallo, et al., "Polarization-entangled photons produced with high-symmetry site-controlled quantum dots," *Nat. Photon.*, vol. 4, no. 5, p. 302, 2010.
[20] L. Anders, C.-W. Hsu, K. F. Karlsson, et al., "Direct generation of linearly polarized photon emission with designated orientations from site-controlled InGaN quantum dots," *Light Sci. Appl.*, vol. 3, no. 1, p. e139, 2014.
[21] P. Michler, *Single Quantum Dots: Fundamentals, Applications and New Concepts*, vol. 90, Springer Science & Business Media, 2003. https://scholar.google.com/scholar_lookup?title=Single%20quantum%20dots%20fundamentals&publication_year=2003&author=P.%20Michler
[22] A. D. Lee, Q. Jiang, M. Tang, Y. Zhang, A. J. Seeds, and H. Liu, "InAs/GaAs quantum-dot lasers monolithically grown on Si, Ge, and Ge-on-Si substrates," *IEEE J. Sel. Top. Quantum Electron.*, vol. 19, no. 4, p. 1901107, 2013.
[23] A. W. Elshaari, I. E. Zadeh, A. Fognini, et al., "On-chip single photon filtering and multiplexing in hybrid quantum photonic circuits," *Nat. Commun.*, vol. 8, no. 1, pp. 1–8, 2017.
[24] P. Bhattacharya, S. Ghosh, and A. D. Stiff-Roberts, "Quantum dot opto-electronic devices," *Annu. Rev. Mater. Res.*, vol. 34, pp. 1–40, 2004.
[25] Y. H. Chang, P. C. Peng, W. K. Tsai, et al., "Single-mode monolithic quantum-dot VCSEL in 1.3 μm with sidemode suppression ratio over 30 dB," *IEEE Photon. Technol. Lett.*, vol. 18, no. 7, pp. 847–849, 2006.
[26] J. J. Dubowski, C. N. Allen, and S. Fafard, "Laser-induced InAs/GaAs quantum dot intermixing," *Appl. Phys. Lett.*, vol. 77, no. 22, pp. 3583–3585, 2000.
[27] S. A. Schwarz, P. Mei, T. Venkatesan, et al., "InGaAs/InP superlattice mixing induced by Zn or Si diffusion," *Appl. Phys. Lett.*, vol. 53, no. 12, p. 1051, 1988.
[28] H. S. Djie, T. Mei, and J. Arokiaraj, "Photoluminescence enhancement by inductively coupled argon plasma exposure for quantum-well intermixing," *Appl. Phys. Lett.*, vol. 83, no. 1, pp. 60–62, 2003.
[29] P. Lever, H. H. Tan, and C. Jagadish, "Impurity free vacancy disordering of InGaAs quantum dots," *J. Appl. Phys.*, vol. 96, no. 12, pp. 7544–7548, 2004.
[30] S. C. Du, L. Fu, H. H. Tan, and C. Jagadish, "Investigations of impurity-free vacancy disordering in (Al) InGaAs (P)/InGaAs quantum wells," *Semicond. Sci. Tech.*, vol. 25, no. 5, 2010, Art no.055014.
[31] H. S. Lee, A. Rastelli, S. Kiravittaya, et al., "Selective area wavelength tuning of InAs/GaAs quantum dots obtained by TiO_2 and SiO_2 layer patterning," *Appl. Phys. Lett.*, vol. 94, no. 16, p. 161906, 2009.
[32] D. Bhattacharyya, A. S. Helmy, A. C. Bryce, E. A. Avrutin, and J. H. Marsh, "Selective control of self-organized in 0.5 Ga 0.5 As/GaAs quantum dot properties: quantum dot intermixing," *J. Appl. Phys.*, vol. 88, no. 8, pp. 4619–4622, 2000.
[33] R. Timm, H. Eisele, A. Lenz, et al., "Structure and intermixing of GaSb/GaAs quantum dots," *Appl. Phys. Lett.*, vol. 85, no. 24, pp. 5890–5892, 2004.
[34] H. S. Lee, K. H. Lee, J. C. Choi, H. L. Park, T. W. Kim, and D. C. Choo, "Enhancement of the activation energy in coupled CdTe/ZnTe quantum dots and quantum-well structures with a ZnTe thin separation barrier," *Appl. Phys. Lett.*, vol. 81, no. 20, pp. 3750–3752, 2002.
[35] A. L. Ankudinov, B. Ravel, J. J. Rehr, and S. D. Conradson, "Real-space multiple-scattering calculation and interpretation of x-ray-absorption near-edge structure," *Phys. Rev. B*, vol. 58, pp. 7565–7576, Sep. 1998.
[36] H. S. Djie, O. Gunawan, D.-N. Wang, B. S. Ooi, and J. C. M. Hwang, "Group-iii vacancy induced $In_xGa_{1-x}As$ quantum dot interdiffusion," *Phys. Rev. B*, vol. 73, p. 155324, Apr. 2006.
[37] T. Takahashi and S. Watanabe, "Recent progress in CdTe and CdZnTe detectors," *IEEE Trans. Nucl. Sci.*, vol. 48, no. 4, pp. 950–959, 2001.
[38] M. T. Man and H. S. Lee, "Discrete states and carrier-phonon scattering in quantum dot population dynamics," *Sci. Rep.*, vol. 5, p. 8267, 2015.
[39] M. T. Man and H. S. Lee, "Clarifying photoluminescence decay dynamics of self-assembled quantum dots," *Sci. Rep.*, vol. 9, p. 4613, 2019.
[40] A. Walsh, L. Juarez, F. Da Silva, and S.-H. Wei, "Origins of band-gap renormalization in degenerately doped semiconductors," *Phys. Rev. B*, vol. 78, Aug. 2008, Art no.075211.
[41] J. D. Ye, S. L. Gu, S. M. Zhu, et al., "Fermi-level band filling and band-gap renormalization in Ga-doped ZnO," *Appl. Phys. Lett.*, vol. 86, no. 19, p. 192111, 2005.
[42] M. T. Man and H. S. Lee, "Carrier transfer and thermal escape in CdTe/ZnTe quantum dots," *Opt. Express*, vol. 22, no. 4, pp. 4115–4122, 2014.

[43] O. Labeau, P. Tamarat, and B. Lounis, "Temperature dependence of the luminescence lifetime of single CdSe/ZnS quantum dots," *Phys. Rev. Lett.*, vol. 90, no. 25, p. 257404, 2003.

[44] P. Cusumano, B. S. Ooi, A. S. Helmy, et al., "Suppression of quantum well intermixing in GaAs/AlGaAs laser structures using phosphorus-doped SiO_2 encapsulant layer," *J. Appl. Phys.*, vol. 81, no. 5, pp. 2445–2447, 1997.

Supplementary Material: The online version of this article offers supplementary material (https://doi.org/10.1515/nanoph-2020-0482).